Theoretical description of electronic properties of vertical gated quantum dots

S. Bednarek, B. Szafran, and J. Adamowski*
Faculty of Physics and Nuclear Techniques, University of Mining and Metallurgy (AGH), Cracow, Poland
(Received 15 May 2001; published 12 October 2001)

A computational method for studying the electronic properties of vertical gated quantum dots is presented. This method is based on the self-consistent procedure of the solution of the three-dimensional Poisson-Schrödinger problem for few-electron systems confined in the quantum dots. In the present paper, we have applied this method to a quantitative description of transport spectroscopy [S. Tarucha *et al.*, Phys Rev. Lett. **77**, 3613 (1996) and L.P. Kouwenhoven *et al.*, Science **278**, 1788 (1997)] in vertical gated quantum dots of the cylindrical symmetry. For the entire nanodevice we have obtained the realistic profile of the confinement potential from the Poisson equation. This potential takes into account all the voltages applied to the leads, the spatial distribution of the ionized donors, and number N of electrons confined in the quantum dot. For small N the calculated lateral confinement potential is approximately parabolic, which supports the previous conjectures that the two-dimensional harmonic-oscillator model can be used for a qualitative description of the gated quantum dots. The present study shows that the approximate parabolicity of the lateral confinement potential is a nontrivial property, since it results from a summation of nonparabolic contributions. The nonparabolic corrections should be included in order to obtain an accurate quantitative description of the transport-spectroscopy data. We have solved the N-electron Schrödinger equation by the unrestricted Hartree-Fock method and calculated the chemical potential for the electrons confined in the gated quantum dot. The chemical potential is found to be a nonlinear function of the gate voltage. We have determined the conversion factor, relating the gate voltage with the energy scale, which enabled us to perform a direct quantitative comparison of the computational results with the experimental data. The present results very well reproduce the measured positions of the current peaks for small source-drain voltage. In particular, we have quantitatively described the shell filling and Hund's rule for artificial atoms. We have also determined the conditions of the single-electron tunneling as functions of the source-drain voltage and the gate voltage and obtained the boundaries of the Coulomb diamonds on the stability diagram. The calculated positions, sizes, and shapes of the Coulomb diamonds are in a very good agreement with experiment. We have also evaluated the distribution of the ionized donors and the surface charge induced on the gate and discussed the problem of screening of interelectron interactions in the quantum dot by the electrodes.

DOI: 10.1103/PhysRevB.64.195303 PACS number(s): 73.21.−b

I. INTRODUCTION

A gated quantum dot (QD) can bind excess electrons in a confinement potential tuned by external voltages applied to the electrodes. The bound electrons form atomiclike bound states, called artificial atoms.[1] The discrete energy levels of artificial atoms can be detected by a transport spectroscopy,[2] which is based on single-electron tunneling. The vertical gated QD was fabricated and studied by transport spectroscopy by Tarucha *et al.*,[3] who obtained beautiful evidence for the shell filling in the artificial atoms. This study was extended[3,4] to a nonzero bias and external magnetic field was applied to the QD. In a recent paper,[5] electron cotunneling has been studied in gated rectangular QD's. The spectacular results obtained by the groups of Tarucha[3] and Kouwenhoven[4] have been quantitatively interpreted in our paper.[6] In other theoretical papers,[7–15] the electronic properties of the gated vertical QD's were studied mainly qualitatively with the use of the fixed confinement potential, i.e., independent of the external electric fields and the number of electrons confined in the QD.

Besides the interesting physics of the single-electron transport phenomena, the nanodevice[3] is a prototype of a single-electron transistor.[16] The source, drain, and gate electrodes attached to the vertical QD (Ref. 3) allow to modify the single-electron tunneling through the QD, which leads to a transistor operation of the nanodevice. The single-electron transistor[3] is in the on state if the chemical potential of electrons confined in the QD falls into a transport window,[17] i.e., takes on the values from the interval defined by the electrochemical potentials of the source and drain. Then, the single-electron tunneling takes place from the source via the QD to the drain. By changing the gate voltage we can reduce the tunneling current to zero, i.e., we can switch off the transistor. The off state of the single-electron transistor corresponds to the quantum Coulomb blockade,[18] which results from a misfit between the discrete energy levels (chemical potentials) of the artificial atom and the transport window. The operation of the single-electron transistor can be explained by the quantum mechanics that allow us to determine the energy levels of the confined electrons and the conditions of the single-electron tunneling.

Several theoretical attempts[7–15] were undertaken in order to describe the vertical gated QD. In Refs. 7, 8, 11, and 12, a two-dimensional model with a parabolic confinement potential was assumed. The three-dimensional confinement potential of the anisotropic harmonic oscillator was used in Refs. 9 and 15. The effects of both the anisotropic harmonic-oscillator potential and the anharmonic corrections were studied in Ref. 13. Nagaraja *et al.*[10] solved the Schrödinger

and Poisson equations for a model perpendicular nanostructure with two electrodes attached and obtained a qualitative description of the shell filling. The qualitative picture of the shell filling has also been obtained by Steffens *et al.*[12] and Rontani *et al.*[14] However, to the best of our knowledge, only in our study[6] was the Poisson-Schrödinger problem solved for the real QD nanostructure[3] with all the voltages applied to the electrodes taken into account, which allowed us to obtain a quantitative agreement with the experimental data.[3,4]

The previous paper[6] was a preliminary announcement of our results for the vertical gated QD. The present paper contains a complete description of the method proposed by us in order to solve the Poisson-Schrödinger problem for the gated QD. Our approach is sufficiently general to be applicable to a three-terminal nanodevice of arbitrary symmetry. Here, we show the application of this method to the vertical gated QD of the cylindrical symmetry.[3,4] Contrary to Ref. 6, in which donor concentrations and layer thicknesses were treated as fitting parameters, in the present paper, we have used the nominal values of these parameters,[19] which we received from the authors.[19] The present calculations, performed with the material data,[19] have led to much better agreement with experiment. In particular, we have obtained 12 Coulomb diamonds (instead of six diamonds as in Ref. 6) in very good agreement with experiment.[4]

The present paper is organized as follows: in Sec. II, we formulate the theoretical method and provide some results, which illustrate our approach, in Sec. III, we present the main numerical results and compare them with the experimental data, Sec. IV contains a discussion, and in Sec. V is found a summary.

II. THEORY

A. Real and model nanostructure

The real nanostructure[3] was fabricated from the multilayer GaAs/AlGaAs/InGaAs heterostructure. It consists of a QD region made of $In_{0.05}Ga_{0.95}As$, which is surrounded by two $Al_{0.22}Ga_{0.78}As$ barriers and a ring-shaped Schottky gate. Each barrier adheres to an undoped GaAs spacer layer, close to which there are stepwise doped *n*-GaAs layers. The *n*-GaAs layers are terminated by the heavily doped GaAs layers (with the donor concentration 2×10^{18} cm^{-3}), which form Ohmic contacts, i.e., the drain (top) and the source (bottom) electrodes.[3] The nanostructure was etched to form a cylindrical pillar to a plane just below the lower (thinner) AlGaAs barrier. The nanostructure is asymmetric with respect to the $z=0$ plane (the z coordinate is measured along the cylinder axis and $z=0$ corresponds to the center of the InGaAs layer). The upper part of the nanodevice is the cylindrical pillar and the lower (substrate) part consists of the nonetched GaAs layers. However, all the experimental results,[3,4] in particular, the Coulomb diamonds on the stability diagram,[4] are almost perfectly symmetric with respect to the drain-source polarity. Therefore, we apply the model nanostructure, which is nearly symmetric with respect to the $z=0$ plane, but we take into account the different widths of the AlGaAs barriers.[3,4,19] In the model nanostructure (Fig. 1), the pillar has been replaced by the mirror reflection of the substrate part of the nanodevice. Therefore, the *n*-GaAs layers and the gate electrode are expanded up to infinity, which enables us to put the boundary conditions needed for a solution of the Poisson equation. In the present work, we have taken on the nominal values[19] of layer thicknesses, donor concentrations, and material compositions.

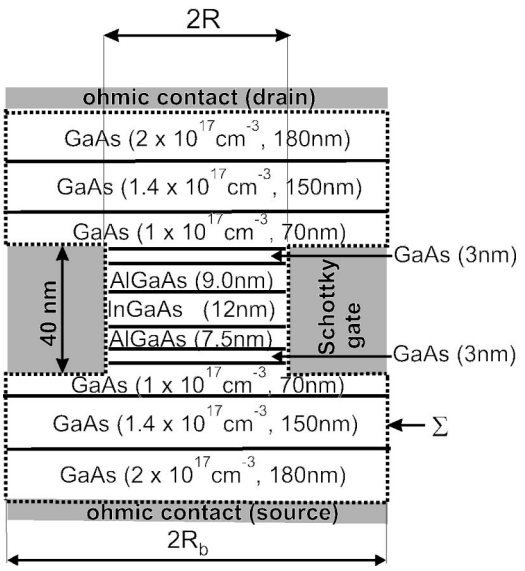

FIG. 1. Schematic of the model nanodevice. Given are the donor concentrations and layer thicknesses, used in the calculations. The boundary conditions for the Poisson equation are put on surface Σ with outer radius R_b. R is the inner radius of the gate.

B. Artificial atom

Excess electrons confined in the QD form atomiclike bound states with discrete energy levels. Therefore, the QD with the confined electrons can be treated as an artificial atom.[1] The number of the confined electrons depends on the depth and range of the confinement-potential well. These parameters determine the so-called ''quantum capacity''[20] of the dot. The characteristic features of electronic shells of the artificial atom are determined by the symmetry and profile of the potential confining the electrons. In the present work, we solve the eigenvalue problem for the many-electron artificial atom by the Hartree-Fock (HF) method. According to this approach, each electron in the QD is subjected to the self-consistent field stemming from the other electrons confined in the QD and the confinement with potential energy $U_{conf}(\mathbf{r})$, which is treated as the potential energy of an external field. The electron confinement results from the double AlGaAs/InGaAs/AlGaAs barrier, which limits the electron motion in the z direction, and electrostatic potential $\varphi_1(\mathbf{r})$, which stems from all the charges in the nanodevice, excluding the charge confined in the QD. In particular, potential $\varphi_1(\mathbf{r})$ gives rise to a lateral confinement. The resulting potential energy of the electron confined in the QD can be written as

$$U_{conf}(\mathbf{r})=U_{db}(z)+U_1(\mathbf{r}), \tag{1}$$

where $U_{db}(z)$ is the double-barrier potential energy, $U_1(\mathbf{r}) = -e\varphi_1(\mathbf{r})$, and $e>0$ is the elementary charge.

C. Electrostatic field and its sources

We aim to solve the complex many-electron quantum-mechanical problem in three-dimensional space. In order to make this problem tractable we separate out the excess electrons confined in the QD, which are treated in the framework of quantum mechanics, from the other sources of the electric field, which are calculated from the Poisson equation. The total electrostatic field in the nanodevice is a superposition of the fields stemming from both kinds of sources. The electrons confined in the QD give rise to the electrostatic potential $\varphi_2(\mathbf{r})$, while the other sources contribute to $\varphi_1(\mathbf{r})$. The total electrostatic potential in the nanodevice is given by the sum

$$\varphi_{tot}(\mathbf{r}) = \varphi_1(\mathbf{r}) + \varphi_2(\mathbf{r}). \tag{2}$$

Both the components of potential (2) originate from the different sources and play diverse roles in the HF method. Therefore, they will be calculated separately and with different accuracy. Potential $\varphi_2(\mathbf{r})$ is calculated with the use of one-electron wave functions $\psi_\nu(\mathbf{r})$ obtained from the HF procedure, i.e.,

$$\varphi_2(\mathbf{r}) = -\frac{e}{4\pi\varepsilon_0\varepsilon_s}\sum_{\nu=1}^{N}\int d^3r'\frac{|\psi_\nu(\mathbf{r}')|^2}{|\mathbf{r}-\mathbf{r}'|}, \tag{3}$$

where N is the number of excess electrons confined in the QD, the sum runs over all the occupied one-electron states, and ε_s is the static dielectric constant.

Potential φ_1 is calculated from the Poisson equation

$$\nabla^2\varphi_1(\mathbf{r}) = -\frac{\varrho_D(\mathbf{r})}{\varepsilon_0\varepsilon_s}, \tag{4}$$

where $\varrho_D(\mathbf{r})$ is the charge density of the ionized donors. In Eq. (4), we take on ε_s to be the static dielectric constant of GaAs and neglect its changes in the heterostructure, since the sources of the electrostatic field with potential φ_1 are localized within the *n*-GaAs layers. The voltages applied to the gate, source, and drain are included via the boundary conditions (cf. Sec. II D). We put the boundary conditions on total potential $\varphi_{tot}(\mathbf{r})$ and calculate the boundary values of potential $\varphi_1(\mathbf{r})$ from Eq. (2). This is an important step, resulting in the avoidance of computational problems, which are inherent in another possible approach[23] based on image charges of the QD-confined electrons. The present approach allows us to incorporate (with controllable precision) all the quantities that determine the distribution of electrostatic field in the nanodevice.

In the nanodevice,[3] we can distinguish two parts, separated by the double tunnel barrier, consisting of the donor-doped GaAs layers attached to the two leads. The source and drain Ohmic contacts are made of the heavily doped *n*-GaAs layers. This means that the donor energy level is aligned with the electrochemical potential, $\mu_{s(d)} = F - eV_{s(d)}$, of the source (drain), where F is the common Fermi energy of the source and drain. The ionized-donor charge density, needed to solve Eq. (4), is determined by the donor ionization condition, which can be derived as follows. We assume that the electron bound to the donor center at position $\mathbf{r}$ in the *n*-GaAs layer can be removed to an adjacent reservoir (source or drain) if the total potential energy of the electron

$$U_{tot}(\mathbf{r}) = -e\varphi_{tot}(\mathbf{r}) \tag{5}$$

exceeds the electrochemical potential of the reservoir. Therefore, we neglect the thermal ionization of the donors. This assumption is justified, since the experiments[3] on the vertical gated QD's were performed at low temperatures (the electron temperature was estimated to be ~ 0.2 K). In this paper, we take the common Fermi energy, F, of the source and drain as the reference energy, which leads to the following formula for the charge density of the ionized donors:

$$\varrho_D(\mathbf{r}) = \begin{cases} en_D(\mathbf{r}), & \text{if } U_{tot}(\mathbf{r}) > -eV_{s(d)}, \\ 0, & \text{otherwise,} \end{cases} \tag{6}$$

where $n_D(\mathbf{r})$ is the donor concentration. We assume that the donors are uniformly distributed within the *n*-GaAs layers and approximate their concentration by stepwise continuous distribution (cf. Fig. 1). Throughout the present paper, the potential of the source is set equal to zero.

D. Boundary conditions

In view of the arguments given in Sec. II C, we put the boundary conditions on the total potential [Eq. (2)] on surface Σ (Fig. 1) and calculate the boundary values of potential $\varphi_1(\mathbf{r})$ from Eq. (2). Accordingly, the boundary conditions take the form

$$\varphi_{tot}(\mathbf{r}_s) = V_s = 0 \tag{7}$$

for the source and

$$\varphi_{tot}(\mathbf{r}_d) = V_d = V_{ds} \tag{8}$$

for the drain, where V_{ds} is the drain-source voltage. Since the metal gate is in contact with the undoped semiconductor layers, we take into account a Schottky barrier of height ϕ_B at the metal-semiconductor interface. Therefore,

$$\varphi_{tot}(\mathbf{r}_g) = V_g - \phi_B/e, \tag{9}$$

where V_g is the gate voltage. In Eqs. (7), (8), and (9), $\mathbf{r}_s$, $\mathbf{r}_d$, and $\mathbf{r}_g$ are the position vectors of the points on the surfaces of the source, drain, and gate, respectively. As the electrodes do not form the closed surface, which surrounds a domain of the solution of the Poisson equation, we enclose this domain with the cylindrical surface, which has the lower and upper base placed on the internal surfaces of the source and drain, respectively (cf. Fig. 1). The outer radius of this cylindrical surface is denoted by R_b. The values of potential $\varphi_1(R_b, z)$ provide the boundary conditions for Eq. (4). In the limit $R_b \to \infty$, the electrostatic field between the source and drain is parallel to the z axis due to the planar structure of the *n*-GaAs layers. In this case, we can determine the boundary conditions for Eq. (4) from the one-dimensional Poisson equation

$$\frac{d^2}{dz^2}\varphi_1(R_b,z) = -\frac{\varrho_D(R_b,z)}{\varepsilon_0\varepsilon_s}. \tag{10}$$

The boundary conditions for Eq. (10) are reduced to putting the values of φ_1 in the two points lying on the internal surfaces of electrodes. We determine these boundary conditions with the help of Eq. (2) and the values of φ_{tot} given by Eqs. (7), (8), and (9) with the left-hand sides taken at points (R_b,z_s), (R_b,z_d), and (R_b,z_g), where z_s, z_d and z_g, are the z coordinates of the source, drain, and gate, respectively. Because condition (6) links the right-hand side of Eq. (10) with the potential, Eq. (10) has to obey the additional condition, which is obtained as follows. The negative external gate voltage leads to the ionization of donors in accordance with condition (6). The ionized donors weaken the effect of the applied voltage and—as a result—the region of the nanostructure, in which the donors are ionized, has a finite extension. The corresponding range (ζ_s and ζ_d) of the ionization of the donors (measured from the dot center towards the source and drain) is implicitly defined by the two conditions, which—for the source—take on the form

$$\varphi_{tot}(R_b,\zeta_s) = 0 \tag{11}$$

and

$$\frac{d}{dz}\varphi_{tot}(R_b,z)\big|_{z=\zeta_s} = 0. \tag{12}$$

For the drain, in the first condition, we put

$$\varphi_{tot}(R_b,\zeta_d) = V_{ds}, \tag{13}$$

while in the second condition [Eq. (12)] we substitute $z=\zeta_d$. Conditions (11), (12), and (13) mean that the z component of the electric field is fully screened and vanishes outside the region of the ionization of the donors. The solutions of Eq. (10) provide the boundary conditions for Eq. (4). Figure 2 shows the boundary values of potential energy $U_1(R_b,z) = -e\varphi_1(R_b,z)$ as functions of gate voltage V_g and coordinate z. The applied drain-source voltage leads to the asymmetry, which is visible in the inset in Fig. 2. Namely, $U_1(R_b,z)\to 10$ meV for $z\to z_d$.

We assume that the solutions of Eq. (10) are valid for the finite, large enough R_b, which enables us to use the finite computational box in the numerical calculations. The choice of R_b is discussed in Sec. II E.

E. Numerical integration of the Poisson equation

Poisson Eq. (4) has been solved by the finite-difference relaxation method in the cylindrical coordinates (ρ,z) on the two-dimensional mesh $(\rho_i = i\Delta\rho, z_j = j\Delta z)$, where $i=0,1,\ldots,50$ and $j=-100,\ldots,100$. The region of integration has been chosen as follows: $0\leqslant\rho\leqslant R_b$ and $z_d\leqslant z\leqslant z_s$. The numerical integration of the Poisson equation yields the values of potential φ_1 on the mesh, i.e., $\varphi_1(\rho_i,z_j)$. Figure 3 shows the calculated potential energy $U_1 = -e\varphi_1$ as a function of ρ and z coordinates. In order to obtain the total potential energy we have to add to U_1 the double-barrier contribution $U_{db}(z)$ [cf. Eq. (2)]. This potential energy is next used in the HF calculations for the electron system confined in the QD. Since the potential well in $U_{db}(z)$ is narrow, i.e., potential $\varphi_1(\rho,z)$ as a function of z only slightly changes in the QD region, we can neglect the z dependence of potential φ_1 (cf. Fig. 3). In the HF method, it is more convenient to use an analytical formula for the potential. For this purpose we have fitted a polynomial, which interpolates between the numerical values $\varphi_1(\rho,0)$. We have found that the six-order polynomial of the form

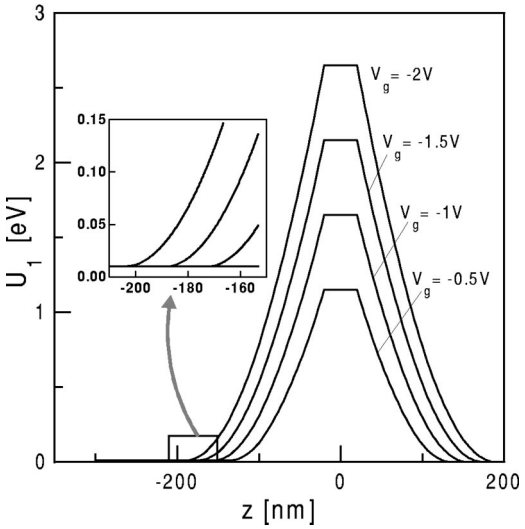

FIG. 2. Boundary conditions for $|V_{ds}| = 10$ mV shown as potential energy $U_1(R_b,z) = -e\varphi_1(R_b,z)$ as functions of coordinate z and gate voltage V_g. The inset shows the enlargement of the region near the drain, in which $U_1\to -eV_{ds} = 10$ meV.

$$\tilde{\varphi}(\rho) = \sum_{m=0}^{3} v_m \rho^{2m} \tag{14}$$

is necessary to fit accurately the numerical solution in the entire QD region, i.e., from the cylinder axis to the gate surface. In Fig. 4, we display the numerical solutions to the Poisson equation, adjusted analytical expression (14), and the parabolic approximations of the numerical solutions fitted in the region occupied by the confined electrons.

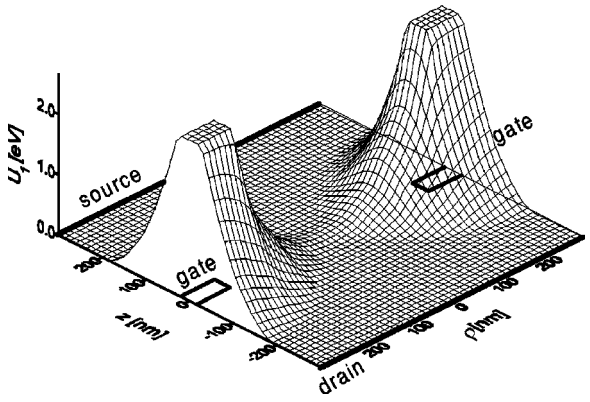

FIG. 3. Potential energy $U_1 = -e\varphi_1$, calculated from the Poisson equation for $V_g = -2$ V, $V_{ds} = 0$, and $N = 0$, as a function of cylindrical coordinates ρ and z.

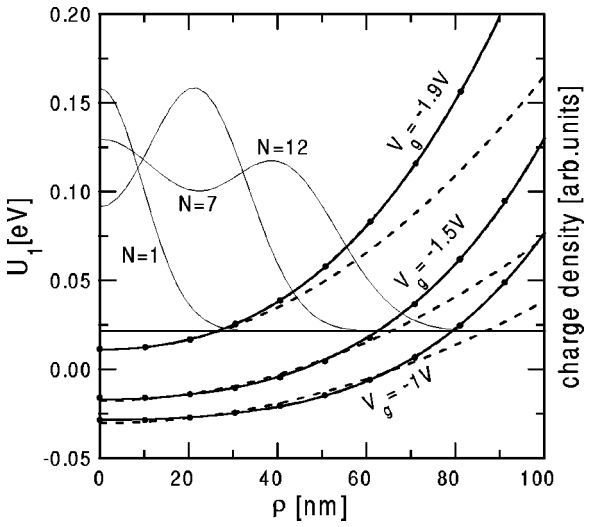

FIG. 4. Potential energy $U_1=-e\varphi_1$ obtained from the numerical solution (dots) of the Poisson equation, the sixth-order polynomials (solid curves), fitted to all the numerical solutions, and the parabolic fits (dashed curves), adjusted to the numerical solutions lying below the shifted Fermi energy F_0, as functions of ρ and V_g for $V_{ds}=0$. The QD confines $N=1$, 7, and 12 electrons for $V_g=-1.9$ V, -1.5 V, and -1 V, respectively. Thin solid curves show the charge density (in arbitrary units) associated with N electrons confined in the QD. Solid horizontal line is drawn at energy F_0, i.e., the Fermi energy of the leads decreased by the space-quantized ground-state energy of the one-electron motion in the z direction.

Figure 5 shows the dependence of coefficients v_0 and v_1 of polynomial (14) on radius R_b, at which we put the boundary conditions when solving the Poisson equation (cf. Sec. II D). In the interval $R_b>300$ nm, these coefficients are almost independent of R_b, which allows us to determine the actual value of R_b. In the present calculations, we have taken $R_b=350$ nm. We have checked that taking $R_b>350$ nm does not change the coefficients in Eq. (14) within the accuracy of four decimal digits.

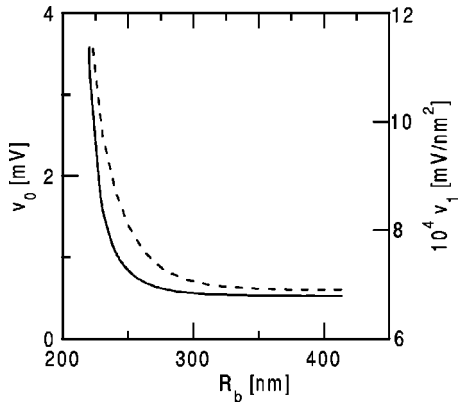

FIG. 5. Coefficients v_0 (solid curve, left scale) and v_1 (dashed curve, right scale) of adjusted polynomial [Eq. (14)] as functions of outer radius R_b of surface Σ, on which we put the boundary conditions for the Poisson equation.

F. Hartree-Fock method

The N-electron Schrödinger equation has been solved by the unrestricted HF method. For the sake of completeness, we briefly describe this method. The HF equations have the form

$$F_s\psi_{ns}(\mathbf{r})=\epsilon_{ns}\psi_{ns}(\mathbf{r}), \tag{15}$$

where F_s are the Fock operators, $\psi_{ns}(\mathbf{r})\equiv\psi_\nu(\mathbf{r})$ are the one-electron wave functions, n denotes the set of orbital quantum numbers, and s is the spin quantum number ($s=\alpha,\beta$, where $\alpha=+1/2$ and $\beta=-1/2$). The Fock operators possess the forms

$$F_\alpha=h+\sum_{n=1}^{N^+}(J_{n\alpha}-K_{n\alpha})+\sum_{m=1}^{N^-}J_{m\beta} \tag{16}$$

and

$$F_\beta=h+\sum_{n=1}^{N^-}(J_{n\beta}-K_{n\beta})+\sum_{m=1}^{N^+}J_{m\alpha}, \tag{17}$$

where h is the one-electron Hamiltonian of noninteracting electrons, and N^+ and N^- denote the numbers of electrons with spin $+\hbar/2$ and $-\hbar/2$, respectively. The Coulomb (J_{ms}) and exchange (K_{ms}) operators are defined by the formulas

$$J_{ms}(\mathbf{r}_i)\psi_{ns}(\mathbf{r}_i)=\left[\int d^3r_j\psi^*_{ms}(\mathbf{r}_j)\frac{e^2}{4\pi\varepsilon_0\varepsilon_\infty r_{ij}}\psi_{ms}(\mathbf{r}_j)\right]\psi_{ns}(\mathbf{r}_i) \tag{18}$$

and

$$K_{ms}(\mathbf{r}_i)\psi_{ns}(\mathbf{r}_i)=\left[\int d^3r_j\psi^*_{ms}(\mathbf{r}_j)\frac{e^2}{4\pi\varepsilon_0\varepsilon_\infty r_{ij}}\psi_{ns}(\mathbf{r}_j)\right]\psi_{ms}(\mathbf{r}_i), \tag{19}$$

where $r_{ij}=|\mathbf{r}_i-\mathbf{r}_j|$ is the interelectron distance. The interaction between the electrons confined in the QD is screened by a high-frequency dielectric constant ε_∞.[22] Contrary to the electrostatic field [cf. Eq. (3)] that mainly acts outside the QD, the electron-electron interaction is not screened by LO phonons.[22]

In the effective-mass approximation

$$h=-\frac{\hbar^2}{2m_e}\nabla^2+U_{ext}(\mathbf{r}), \tag{20}$$

where the potential energy of the electron in the external field is taken to be [cf. Eq. (1)]

$$U_{ext}(\mathbf{r})=U_{conf}(\mathbf{r})=U_{db}(z)-e\tilde{\varphi}(\rho), \tag{21}$$

and potential $\tilde{\varphi}$ is defined by Eq. (14). The HF equations have been solved by variational means with one-electron wave functions expanded in the Gaussian basis,

$$\psi_{ns}(\mathbf{r})=\sum_{pqr}c_{ns}^{pqr}g_{pqr}(x,y,z), \tag{22}$$

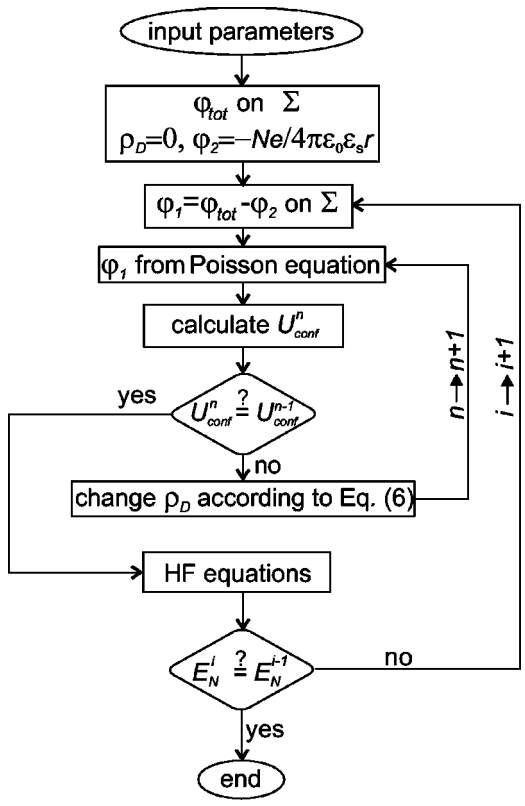

FIG. 6. Block diagram of the self-consistent Poisson-Hartree-Fock procedure. A detailed description is given in the text.

where

$$g_{pqr}(x,y,z)=x^p y^q \exp[-\alpha_r(x^2+y^2)-\beta z^2], \qquad (23)$$

c_{ns}^{pqr}, α_r, and β are the variational parameters, and the sums run over $p,q=0,1,\ldots,$ $p+q\leqslant 4$, and $r=1,2,3$.

G. Self-consistent procedure

We use the solutions of the HF equations to calculate total energy E_N of the N-electron system confined in the QD. Energy E_N depends on the profile of the electrostatic potential in the nanodevice, which is affected by the distribution of the ionized donors in n-GaAs layers. The systems of the electrons confined in the QD and the ionized donors in the n-GaAs layers are coupled by the Coulomb interaction. Because of the mutual dependence of the density of the confined electrons and the distribution of the ionized donors [cf. condition (6)], the Poisson-Schrödinger problem for the entire nanodevice has to be solved self-consistently. For this purpose we have applied the iterative procedure depicted in the block diagram (Fig. 6). In Fig. 6, the two iteration loops are displayed. In the inner loop (labeled n), we calculate charge density ϱ_D of the ionized donors and electrostatic potential φ_1 for a given distribution of the confined charge carriers. The inner loop is terminated if the self-consistency of the confinement-potential energy [Eq. (1)] is reached. The outer loop (labeled i) assures the self-consistency of the charge distribution of the electrons confined in the QD and the electrostatic potential in the nanodevice. In the first step of the iterative procedure, the distribution of the confined charge carriers is taken on to be that of the point charge of N electrons, i.e., $\varphi_2=-Ne/4\pi\varepsilon_0\varepsilon_s r$. The Poisson equation is solved for the electrostatic potential in the entire nanodevice, which allows us to determine the distribution of the ionized donors in the n-GaAs layers. Next, the calculated confinement potential is used as the external potential in the HF equations. The solutions of the HF equations enable us to calculate the N-electron energy E_N and the confined charge-carrier distribution. The last quantity is reintroduced into the Poisson equation. The iterations run until a convergence of E_N is reached. The convergence of the present procedure is very fast, in particular, the outer loop has to be executed two or three times only.

H. Conditions of the single-electron tunneling

The transport-spectroscopy measurements[3] are based on single-electron tunneling via the nanostructure. The conditions of the single-electron tunneling[24,25] are determined by the electrochemical potentials of the source (μ_s) and drain (μ_d) and the chemical potential of the electrons confined in the QD, which is defined as

$$\mu_{N+1}=E_{N+1}-E_N. \qquad (24)$$

A single electron can tunnel from the source to the drain through the QD that contains N bound electrons, if[24,25]

$$\mu_s \geqslant \mu_{N+1} \geqslant \mu_d. \qquad (25)$$

At the reverse bias, i.e., $V_{ds}<0$, the electron can tunnel from the drain to source. Then, in condition (25), the signs of inequalities have to be changed. During the single-electron tunneling process the number of excess electrons localized in the QD fluctuates as follows: $N\rightarrow N+1\rightarrow N\rightarrow\cdots$. If conditions (25) are not fulfilled, the flow of current is blocked, i.e., we deal with the quantum Coulomb blockade.[18] Due to the equality signs in condition (25), the single-electron tunneling can occur even at zero drain-source voltage. Then,

$$\mu_s=\mu_{N+1}=\mu_d. \qquad (26)$$

This condition allows us to determine the positions of current peaks measured for $V_{ds}\simeq 0$.

I. Parameters of the model nanostructure

In the present paper, we have used the nominal values[19] of the layer thicknesses and donor concentrations in the nanostructure (cf. Fig. 1). Moreover, we have taken on the electron effective mass of $In_{0.05}Ga_{0.95}As$ to be[26] 0.0643 of the electron rest mass and neglected the small jump of the electron effective mass at the InGaAs/AlGaAs interface, since the electron bound-state wave function very weakly penetrates into the barrier region. We neglect the changes of dielectric constants at the interfaces and take $\varepsilon_s=13.2$ appropriate for GaAs (Ref. 27) and $\varepsilon_\infty=11$ for $In_{0.05}Ga_{0.95}As$.[28] The height of the Schottky barrier at the GaAs/metal interface ϕ_B is taken to be 0.65 eV.[29] The shape of the double-barrier potential energy $U_{db}(z)$ in the GaAs/AlGaAs/InGaAs heterostructure is given by

$$U_{db}(z)=\begin{cases}0, & \text{for the GaAs spacers,}\\ U_b, & \text{for the } Al_{0.22}Ga_{0.78}As \text{ barriers,}\\ U_w, & \text{for the } In_{0.05}Ga_{0.95}As \text{ quantum dot.}\end{cases} \tag{27}$$

In the calculations, we have taken $U_b=240$ meV (Ref. 27) and $U_w=-59$ meV, estimated from the gap difference.[30] We have checked that the change of U_w within physically acceptable limits does not change the relative values of the calculated chemical potentials, which—according to Eq. (26)—determine the positions of current peaks.

Since the cylindrical pillar has been obtained in the etching process,[16] the inner radius R of the gate cannot be accurately measured. Before the etching process[16] the nanostructure was covered with the circular drain of the radius $R_d=250$ nm. Inner gate radius R has to be smaller than the drain radius, i.e., $R<R_d$, which accounts for an undercut in the cylindrical pillar.[3] In the present calculations, we have adjusted the value of R in order to reproduce the exact positions of the current peaks measured[3] as a function of the gate voltage at the small drain-source voltage. For this purpose we proceed as follows: according to condition (26) of the single-electron tunneling at $V_{ds}=0$, we calculate chemical potentials μ_N for $N=1,\ldots,12$ and for the gate-voltage values $V_g(N)$ that correspond to the measured current peaks at the small bias.[3] Therefore, N simultaneously denotes the subsequent number of the current peak. If the gate radius has the correct value, calculated chemical potentials μ_{N+1} are equal to the common Fermi energy of the source and drain, i.e., the chemical potential is independent of N. For the incorrectly chosen value of R, condition (26) is not fulfilled. The dependence of the calculated chemical potential on N is shown in Fig. 7 for $R=220.0$ nm (crosses), 223.4 nm (circles), and 226.0 nm (triangles). In Fig. 7, the circles can be approximately aligned on the horizontal straight line. In this case, the chemical potential of the QD-confined electrons is independent of N, which allows us to determine the inner gate radius. In the following, we take $R=223.4$ nm.

In Fig. 7, the left energy scale corresponds to the results obtained with the potential-well depth U_w [Eq. (27)] taken as the band-gap difference,[30] which corresponds to 100% conduction-band offset. Under this assumption, the mean value of the calculated chemical potentials is placed 9.5 meV below the conduction-band minimum of the GaAs spacer. This value determines the relative position of the Fermi level. However, the Fermi level should be located at the donor energy level, i.e., 5.8 meV below the GaAs conduction-band bottom. Therefore, potential-well depth U_w should be raised by the difference of the above values, which yields $U_w=-55.3$ meV. This value corresponds to 94% conduction-band offset, which is larger than the published values 46%–83% for the InAs/GaAs quantum wells.[31] The larger conduction-band offset for the gated QD can result from the presence of the leads in the nanodevice. We note that this change of the confinement-potential-well depth does not change the relative values of the chemical potentials, i.e., the addition energies. In Fig. 7, the zero is put at the conduction-band bottom of the GaAs spacer on the left scale and is shifted to the Fermi level of the leads on the right scale.

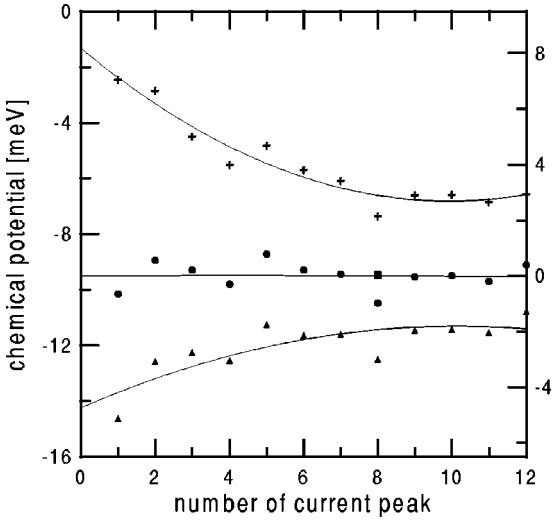

FIG. 7. Chemical potential calculated with the gate-voltage values $V_g(N)$, which correspond to the subsequent current peaks N measured by Tarucha *et al.*[3] The symbols (crosses, circles, and triangles) display the results obtained for $R=220.0$ nm, 223.4 nm, and 226.0 nm, respectively. The square for $N=8$ shows the result obtained under the assumption of tunneling via the first-excited state. Thin solid curves serve as guides for the eye. On the left (right) scale, the zero is at the conduction-band minimum of the GaAs spacer (the common Fermi energy of the source and drain).

Figure 7 also illustrates how sensitive the present results are on the choice of the inner radius of the gate. The small change of R leads to a noticeable upward or downward bending of the $\mu_N[V_g(N)]$ curves.

In Fig. 7, the chemical potential for $N=8$ exhibits the largest deviation from the Fermi energy. However, in this case, the chemical potential calculated for the lowest-energy excited state of the eight-electron system is exactly equal to the Fermi energy (cf. the full square at $N=8$ in Fig. 7). Therefore, we tentatively ascribe the eighth current peak to the tunneling via the first-excited state. A more detailed discussion of this effect is given in Sec. IV.

III. RESULTS

A. Confinement potential

The calculated profile of the total confinement-potential energy (with the double-barrier potential included) is shown in Fig. 8 as a function of cylindrical coordinates ρ and z. Figure 8 provides an illustration of the potential-energy variation in the central part of the nanodevice.

Let us turn back to Fig. 4, which shows the solutions of the Poisson equation as well as the charge density associated with N electrons confined in the QD. Number N of the confined electrons increases with the increasing gate voltage. The confined electrons are localized in the central region of the QD and very weakly penetrate into the region, in which the potential energy exceeds the energies of the occupied

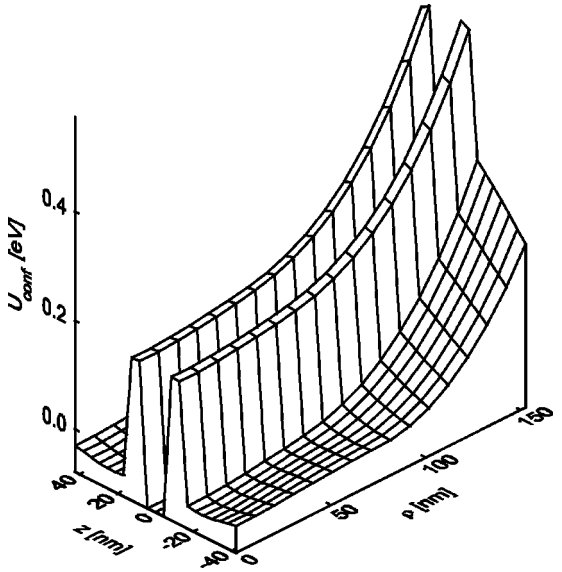

FIG. 8. Confinement-potential energy U_{conf} [Eq. (1)] as a function of cylindrical coordinates ρ and z in the central region of the QD.

one-electron states (cf. thin solid curves in Fig. 4). For $V_{ds}=0$, i.e., $\mu_s=\mu_d=F$, the one-electron energies [Eq. (15)] do not exceed the Fermi energy of the source and drain, i.e., $\epsilon_{ns}\leqslant F$. According to Fig. 4, the movement of the QD-confined electrons is limited to this region of space, in which the potential energy does not exceed the Fermi energy. For the noninteracting electrons the one-electron Schrödinger equation with Hamiltonian (20) and potential energy (21) can be separated into two eigenequations, which describe the in-plane and vertical motion. Thus, the one-electron ground-state energy ϵ_0 is a sum of the lowest eigenvalues $\epsilon_\perp$ and ϵ_z of both the eigenproblems, i.e., $\epsilon_0=\epsilon_\perp+\epsilon_z$. The one-electron wave function is localized within the region approximately limited by the following inequalities: $U_{db}(z)\leqslant\epsilon_z$ in the vertical direction and $U_1(\rho)\leqslant\epsilon_\perp$ in the plane within the InGaAs layer. This means that—on the U_1 vs ρ plot (Fig. 4)—the region in which the electrons are localized can be bounded by the inequality $U_1(\rho)\leqslant F_0$, where $F_0=F-\epsilon_z$ is the Fermi energy decreased by the ground-state energy of the space-quantized motion in the z direction. We have calculated energy ϵ_z, which is independent of the gate voltage and donor concentration, with the variational wave function being the single z-dependent Gaussian. This yields the estimate of $\epsilon_z\simeq 28$ meV above the bottom of the InGaAs potential well, i.e., 27.3 meV below the GaAs conduction-band minimum. According to the discussion given in Sec. III, the Fermi energy lies 5.8 meV below the GaAs conduction-band minimum. The difference of the last two values (21.5 meV) provides the estimate of F_0, which can be interpreted as the maximum value of potential energy $U_1(\rho)$, above which the charge density of the confined electrons vanishes (cf. Fig. 4).

In the region of the localization of electrons, total potential energy U_{tot} [Eq. (5)] also lies below F_0. In this region of the QD, lateral confinement-potential energy $U_1(\rho)$ is an approximately parabolic function of ρ (Fig. 4). Nevertheless,

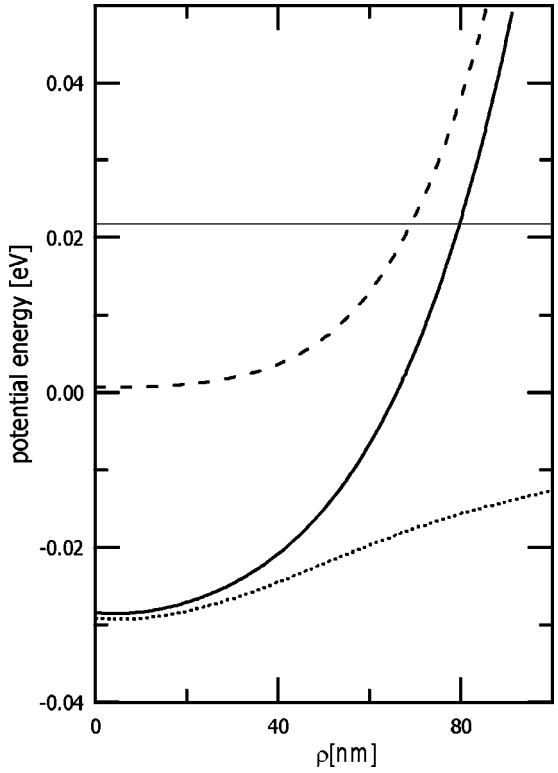

FIG. 9. Potential energy U_1 of the lateral confinement (solid curve) and its two components: the potential energy of the empty QD (dashed curve) and the potential energy resulting from the response of the nanodevice on the presence of $N=12$ electrons in the QD (dotted curve), as functions of radial cylindrical coordinate ρ. The results are displayed for $V_g=-1$ V. Shifted Fermi energy F_0 is depicted by the thin solid line.

the nonparabolicity of $U_1(\rho)$ is also visible in Fig. 4. For a small number of the QD-confined electrons the nonparabolic corrections are noticeable beyond the region occupied by the electrons (cf. the results for $V_g=-1.9$ V in Fig. 4). The nonparabolic corrections start to play a role in a description of QD-confined electrons[32] if the number of electrons exceeds ~ 12. This property, obtained by us from the self-consistent solution of the Poisson equation, is in a full agreement with the conclusions[21] based on experiment.

We have studied the physical origin of the lateral confinement potential in more detail. Figure 9 displays the results for $V_g=-1$ V, which correspond to $N=12$ electrons bound in the QD. Potential φ_1 can be decomposed into the sum of the following two components: (i) the potential created by the leads for $N=0$ and (ii) the potential of the response of the nanodevice on the presence of N electrons in the QD. Component (ii) takes into account the screening of the electrostatic field of the QD-confined electrons by the leads. Figure 9 shows that the approximate parabolicity of the lateral potential energy of the electron is a result of the summation of the two clearly nonparabolic contributions. Therefore, the approximate parabolicity of the lateral confinement potential appears to be a nontrivial and unexpected property.

The effect of the charge confined in the QD on the potential energy is shown in Fig. 10. When varying the gate voltage we change the quantum capacity of the QD.[20] If the gate

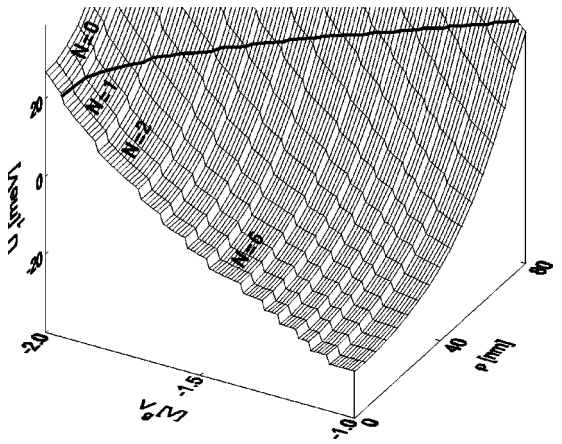

FIG. 10. Potential energy $U_1 = -e\varphi_1$ as a function of gate voltage V_g, radial cylindrical coordinate ρ, and number N of electrons confined in the QD. Thick solid line corresponds to shifted Fermi energy F_0.

voltage increases, taking on the smaller absolute values (Fig. 10), the QD traps the subsequent electrons, which in turn ionize more donors in *n*-GaAs layers. This leads to the stepwise behavior of potential energy U_1 (Fig. 10). Figure 10 shows how strongly the electrons confined in the QD modify the confinement potential. This modification appears to be essential in the operation of the nanodevice.

B. Quantum Coulomb oscillations and Coulomb diamonds

The upper panel of Fig. 11 displays the chemical potential calculated for $V_{ds}=0$. The zero on the energy scale corresponds to the common Fermi energy of the source and drain. According to condition (26), a single electron can tunnel through the nanodevice if the chemical potential of the *N*-electron system confined in the QD is aligned with the source and drain electrochemical potentials. The crossing points of μ_N with the abscissa very well agree with the experimentally measured[3] positions of current peaks, shown by thin vertical lines on Fig. 11. The unequal spacings between the subsequent peaks result from the shell filling of the artificial atoms.[3,4] In particular, in Fig. 11, the distinctly larger separations between the second and third, and the sixth and seventh vertical lines correspond to the filling of the first and the second electronic shell, respectively, while the slightly larger separations between the fourth and fifth, and the ninth and tenth vertical lines correspond to the half filled shells, i.e., Hund's rule.

In the lower panel of Fig. 11, we report the results of the present calculations for the gate-voltage-to-energy conversion factor, which is defined as follows:

$$\alpha_N(V_g) = \left.\frac{\partial \mu_N}{\partial V_g}\right|_{V_{ds}=0}. \tag{28}$$

In Fig. 11, we have plotted α_N vs the gate voltage only for the values of V_g close to the current peak positions. The calculated conversion factor allows us to transform the chemical potential into the gate voltage. Therefore, we are

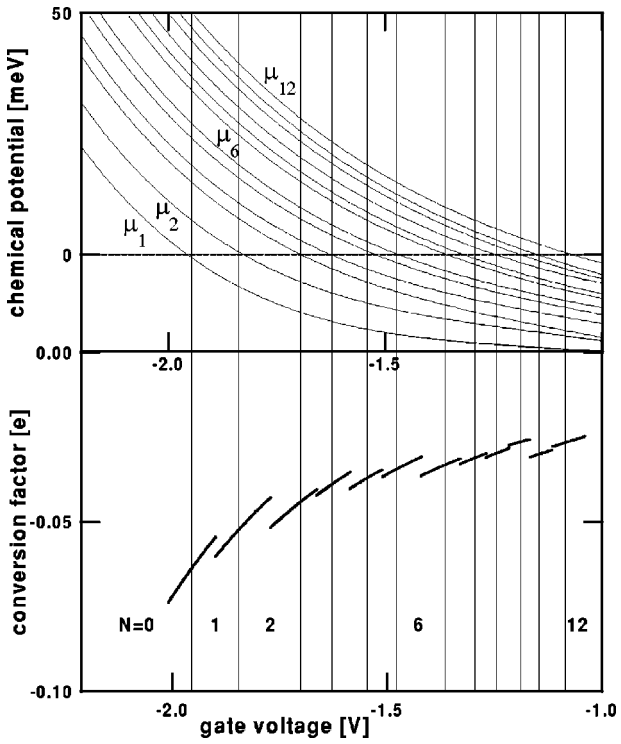

FIG. 11. Chemical potential μ_N, calculated for $V_{ds}=0$ (upper panel), and conversion factor α_N, defined by Eq. (28), plotted as functions of the gate voltage and number N of the electrons confined in the QD. The single-electron tunneling takes place if $\mu_N = F = 0$. The measured positions of current peaks, taken from Ref. 3, are shown by thin vertical lines.

able to perform a direct comparison between the calculated chemical potentials and measured gate voltages, which correspond to the current peaks. The calculated values of the conversion factor show an overall agreement with the experimentally determined values of this quantity.[3,4,21] In particular, the absolute values of α_N decrease with increasing N.[21] However, we note that the experimental values of the conversion factor have been estimated from the geometric sizes of the Coulomb diamonds[4] taken at the nonzero source-drain voltage and under the assumption that half of the applied drain-source voltage is effective at the QD position.

The results for the nonzero drain-source voltage are reported in Fig. 12. The experimental points in the shaded areas correspond to the nonzero differential conductance.[4] The solid curves show the calculated boundaries between the regimes of zero and nonzero conductance. The curves with the positive and negative slope correspond to $\mu_{N+1}=\mu_s$ and $\mu_{N+1}=\mu_d$, respectively. All the solid curves have been obtained for tunneling via the corresponding ground state. The dashed curves display the results obtained under the assumption of tunneling via the first-excited state of the eight-electron system. The calculated boundaries of the Coulomb blockade regions very well agree with the measured positions, sizes, and shapes of the 12 Coulomb diamonds.

C. Induced-charge density

The operation of the nanodevice[3] is strongly dependent on the charge distribution of the ionized donors. This quantity is

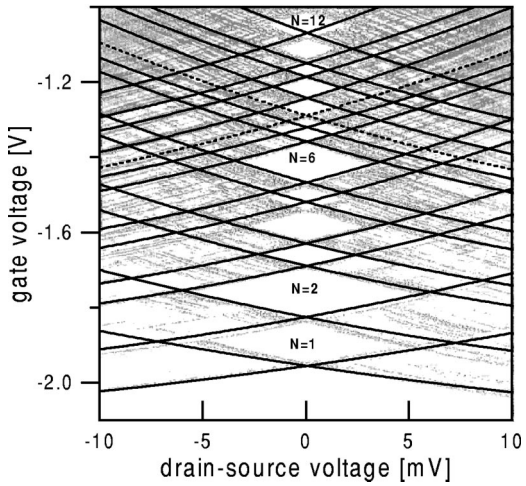

FIG. 12. Stability diagram with Coulomb diamonds. Solid curves show the calculated boundaries of the single-electron tunneling [cf. condition (25)] via the *N*-electron ground states. Dashed curve corresponds to the tunneling of the eighth electron via the first-excited state. Dots (shaded areas) show the experimental data.[4] In the white diamond-shaped regions, the number of the QD-confined electrons is fixed and equal to *N*.

hardly accessible in experiment; however, the present computational method provides a useful tool for determining it. Figures 13(a)–13(d) depict the results of the present calculations. Figures 13(a) and 13(b) show the induced space-charge density for $V_g=-1$ V and $V_g=-2$ V, respectively. In both cases, there are no electrons confined in the QD and $V_{ds}=0$; therefore, the space charge is induced by the gate voltage only. The stepwise increase of the induced-charge density corresponds to the stepwise increasing concentration of donors in the subsequent *n*-GaAs layers. The space, occupied by the ionized donors, extends if the gate voltage is lowered. The effect of the charge confined in the QD is shown in Fig. 13(c). The QD-confined electrons additionally induce the space charge in the central part of the nanodevice. In Figs. 13(a), 13(b), and 13(c), the induced space-charge distribution is almost symmetric with respect to the inversion in the $z=0$ plane. The small difference in the barrier widths causes a slight asymmetry. The pronounced asymmetry of the induced-charge distribution appears under the applied bias. This effect is illustrated in Fig. 13(d) for $V_{ds}=50$ mV. The real nanodevice[3] consists of the three *n*-GaAs layers. The present numerical results show that the donors become ionized in two layers only, i.e., only the two *n*-GaAs layers adjacent to the double-barrier heterostructure effectively screen the electric field in the nanostructure. This conclusion is valid for the nanodevice parameters quoted in Fig. 1.

Having at our disposal the potential profile determined in the entire nanodevice, we can find the surface charge induced at the gate electrode. For this aim, we have solved the inverted Poisson equation, i.e., Eq. (4), in which potential φ_1 is known and the charge density is sought at the gate surface $\mathbf{r}=\mathbf{r}_g$. The calculated surface density of the charge induced at the gate is depicted in Fig. 14. The negative values of the

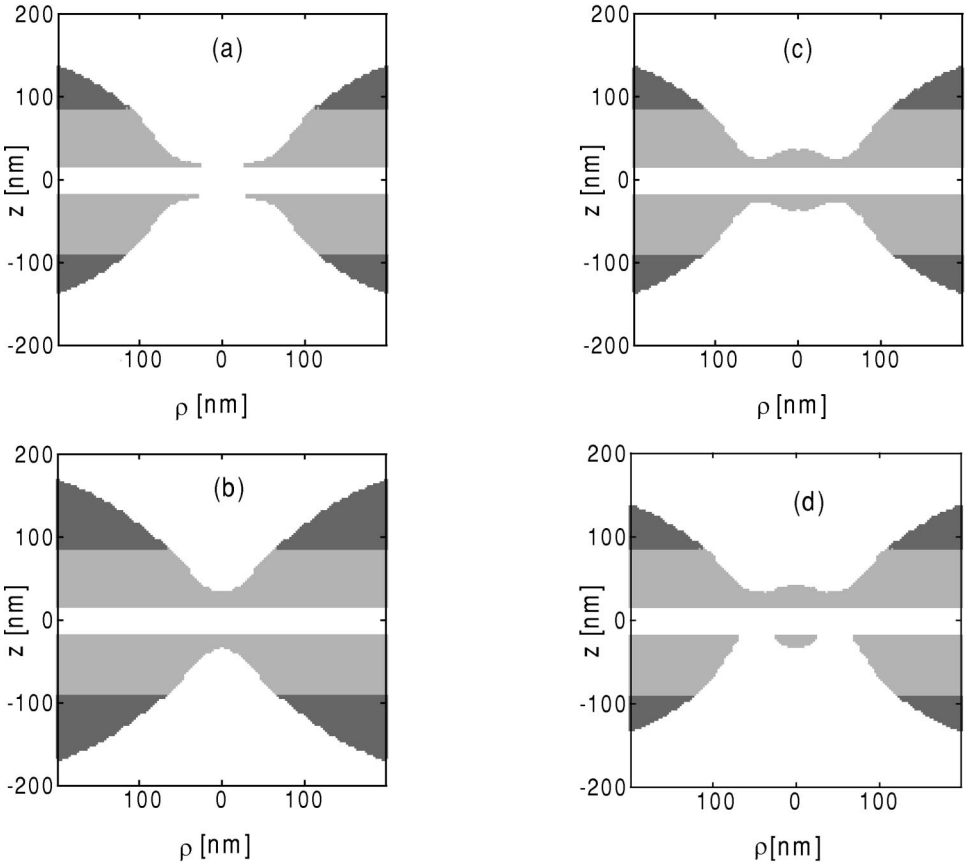

FIG. 13. Ionized-donor charge density induced in *n*-GaAs layers shown in the cross section of the cylindrical nanodevice as a function of cylindrical coordinates ρ and z. The white, grey, and dark grey regions correspond to charge density $\varrho_D=0$, 1×10^{17}, and 1.4×10^{17} $[e/\mathrm{cm}^3]$, respectively. Shown are the results for (a) $V_g=-1$ V, $V_{ds}=0$, $N=0$, (b) $V_g=-2$ V, $V_{ds}=0$, $N=0$, (c) $V_g=-1$ V, $V_{ds}=0$, $N=12$, and (d) $V_g=-1$ V, $V_{ds}=50$ mV, $N=0$. N is the number of electrons confined in the QD region, which is located close to $z=\rho=0$.

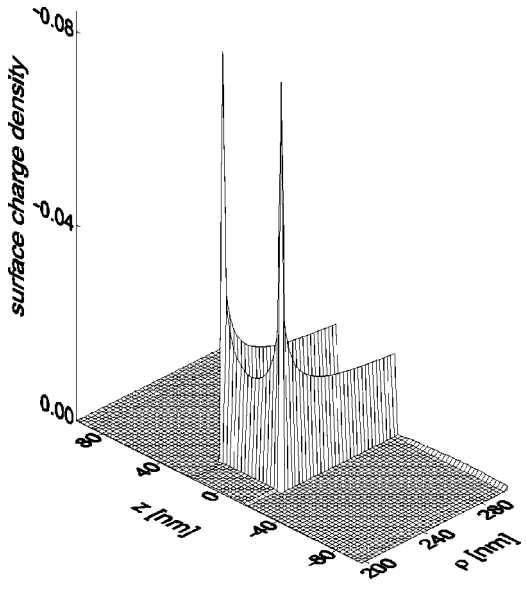

FIG. 14. Surface charge density (in units e/nm^2) of the charge, induced at the surface of the gate, plotted as a function of cylindrical coordinates ρ and z.

induced surface charge assure the charge neutrality of the nanostructure. The characteristic peaks account for the large electric-field gradient at the gate edges.

IV. DISCUSSION

In the present paper, the Schrödinger equation has been solved by the HF method, in which the electron-electron correlation is neglected. In our previous paper,[33] we have quantitatively determined the effect of correlation for the three-dimensional two-electron system in a parabolic isotropic and anisotropic confinement potential. Our study[33] has shown that the HF and exact results very well agree with each other for the QD's of small and intermediate size, which corresponds to the range of the confinement potential up to ~ 100 nm. Taking on the model parabolic anisotropic confinement[33] with the parameters compatible with the vertical gated QD,[3] we have estimated the inaccuracy of the HF ground-state energy to be ~ 1 meV for the two-electron system. It is known that—in the quantum-mechanical calculations for natural atoms—the HF method works better for the atoms with the larger number of electrons. The inaccuracy caused by the neglected electron-electron correlation can be responsible for the small deviations of the calculated chemical potentials from the Fermi energy (cf. Fig. 7).

The chemical potential calculated for the ground state of the eight-electron system exhibits the largest deviation from the Fermi energy. In the eight-electron ground state, the electrons occupy the following spin orbitals: $(1s\uparrow)(1s\downarrow)(1p_+\uparrow)(1p_+\downarrow)(1p_-\uparrow)(1p_-\downarrow)(1d_+\uparrow)(1d_-\uparrow)$, i.e., five spin orbitals with spin up and three spin orbitals with spin down. (The orbitals with the azimuthal quantum number $l=0$, 1, and 2 are denoted by s, p, and d, respectively.) The energy of this ground state is very close to the energy of the first-excited state, in which the following spin orbitals are occupied by the electrons: $(1s\uparrow)(1s\downarrow)(1p_+\uparrow)(1p_+\downarrow)(1p_-\uparrow)(1p_-\downarrow)(1d_+\uparrow)(1d_+\downarrow)$, i.e., four spin orbitals with spin up and four spin orbitals with spin down. The chemical potentials calculated with this first-excited-state energy exactly agree with the Fermi energy of the source and drain (Fig. 7) and lead to a good agreement between the calculated and measured boundaries of the Coulomb diamonds (cf. dashed curves in Fig. 12). This would lead to a suggestion that the eighth electron may tunnel via the first-excited state. However, since no selection rules support this suggestion, this problem requires further study.

The chemical potentials can also be changed by the anisotropy of the nanostructure,[34] which can essentially change the rotational symmetry of the confinement potential.[34] In the perpendicular gated QD's, studied by Austing *et al.*,[34] the confinement potential possesses an ellipsoidal symmetry. However, in the cylindrical QD's,[3] the anisotropy can be treated as a small perturbation, which slightly shifts the chemical potentials for the few-electron systems.[6]

The confinement potential depends on the number of electrons confined in the QD. This leads to the problem of the rate of relaxation of the ionized-donor distribution during single-electron tunneling via the QD. The following question arises: how fast does the ionization of donors follow the change of the number of QD-confined electrons? In order to answer this question we consider two extreme mechanisms of the rapid and slow relaxation during tunneling of the $(N+1)$th electron via the nanodevice. According to the rapid-relaxation mechanism, the donors immediately follow the presence of each additional electron in the system. Therefore, the electronic component of potential [Eq. (3)] should originate from the actual number of the QD-confined electrons. In this case, the energies E_{N+1} and E_N, needed to determine chemical potential [Eq. (24)], should be calculated with the use of the different confinement potentials. We have performed the calculations according to this mechanism and found that the results do not reproduce the tunneling-current peaks correctly.

The slow-relaxation mechanism corresponds to the resonant tunneling. Then, during the flow of the single electron through the QD, the response of the donor system on the change of the number of excess electrons is extremely slow. Therefore, both the energies E_{N+1} and E_N should be calculated with the same confinement potential. In the present paper, we provide the results obtained under assumption of slow relaxation. They are in a very good agreement with experiment. It is interesting that we obtain agreement with experiment if we calculate E_N and E_{N+1} taking the confinement potential for N as well as $N+1$ electrons confined in the QD. In both cases, the chemical potentials are approximately placed on two horizontal straight lines (like the one shown in Fig. 7), which are slightly shifted (by 2 meV) with respect to each other. These results strongly support the slow-relaxation mechanism with the average number of confined electrons between N and $N+1$. Additionally, the lack of hysteresis of the measured current-gate-voltage characteristics[3,4] provides experimental support[21] for the slow-relaxation mechanism.

In the gated nanodevice,[3] screening of the electrostatic potential is very important.[23] The present approach takes the

screening into account via the proper boundary conditions on lead surfaces and the incorporation of the ionization of donors. An alternative (and equivalent) method was proposed by Bruce and Maksym,[23] who considered the gated nanodevice, but with different structure.[35] The authors[23] introduced the image charges in order to take the screening into account and obtained the nonparabolicity of the confinement potential as a result of screening. Contrary to the present paper, the authors[23] considered the nanodevice[35] in which all the donors were ionized. The present approach seems to be simpler, since we obtain the confinement potential directly from the Poisson equation without a need of the additional calculation of the Green function like in Ref. 23.

The present results show that—in the three-electrode nanodevice[3]—it is not possible to account for the screening of the electron interactions within the dot by either a single effective dielectric constant or a single screening function.[36] This screening results from the charge induced by the QD-confined electrons. The induced charge is located too far from the QD region, i.e., in the *n*-GaAs layers and the remote gate electrode (cf. Figs. 13 and 14), in order to be effective in the direct screening of the electron-electron interactions within the QD. The problem of screening in the gated QD's is much more complicated than that of screening via an effective medium. Nevertheless, this complex problem has been solved in the present paper. The calculated response potential (cf. dotted curve in Fig. 9) shows the effect of screening of the interactions between the electrons within the QD by the leads. We have shown that—in the vertical gated QD—the screening depends on external voltages applied to the electrodes, the distribution of ionized donors, and the charge confined in the QD. Therefore, its determination requires the self-consistent solution of the Poisson-Schrödinger problem for the entire nanodevice, which was done in the present work.

The problem of the nonparabolicity of the lateral confinement potential has been discussed in the relation with Figs. 4 and 9. Here, we summarize this discussion by a statement that the lateral confinement potential is almost parabolic below the Fermi level and exhibits the distinct nonparabolicity near and above the Fermi level. Due to the complex electrostatics of the nanodevice, the approximate parabolicity of the lateral confinement potential is an *a priori* unexpected result. As shown in Fig. 9, both the components of the lateral confinement potential are clearly nonparabolic.

In other theoretical papers, agreement with experiment data[3] was claimed for the addition energy, e.g., Ref. 15. However, the addition energy, defined as $\Delta\mu_N=\mu_{N+1}-\mu_N$, can be extracted from the experimental data only if the gate-voltage-energy conversion factor is known. As shown in the lower panel of Fig. 11, the conversion factor strongly depends on the gate voltage and the number of electrons confined in the QD. These effects are neglected if the confinement potential is fixed as in Ref. 15.

In the present paper, good quantitative agreement with experiment[3,4] has been obtained with the use of nominal values[19] of the layer thicknesses and donor concentrations. The values of the effective band masses and dielectric constants have been taken from the literature.[26–28] We have also taken on reliable values of parameters characterizing the AlGaAs/InGaAs/AlGaAs double-barrier heterostructure and checked that the changes of these parameters within physically acceptable limits have a negligible effect on the conditions of the single-electron tunneling via the nanodevice. Only the inner radius of the gate cannot be measured with sufficient precision. Therefore, in the present paper, we had to treat this radius as the adjustable parameter. Figure 7 shows how sensitive the conditions are of the single-electron tunneling on the small changes of the gate radius.

V. SUMMARY

We have elaborated the self-consistent method of the solution of the Poisson-Schrödinger problem for the three-electrode QD-based nanodevice. In the present paper, we have applied this approach to the vertical gated quantum dot of the cylindrical symmetry. The present method has enabled us to determine the three-dimensional profile of the confinement potential, calculated from first principles of electrostatics. We have taken into account the number of electrons confined in the QD, the voltages applied to the leads, and the distribution of the ionized donors. The calculated confinement potential exhibits a complex dependence on these quantities. We have shown that the evaluation of the realistic confinement potential is of crucial importance for an accurate quantitative description of the electronic properties of the nanodevice. We have discussed the problem of nonparabolicity of the lateral confinement potential and the problem of screening of interelectron interactions within the QD. For small N and the energy below the Fermi level the calculated lateral confinement potential is approximately parabolic, which supports the previous conjectures that the two-dimensional harmonic-oscillator model qualitatively describes the properties of the artificial atoms formed in the nanostructure. Nevertheless, the incorporation of the nonparabolic corrections is necessary for an accurate quantitative description. The deviations from the parabolicity become important for large N and the energies near and above the Fermi level. We have also shown that the approximate parabolicity of the lateral confinement potential results from the summation of the two clearly nonparabolic contributions. One of the components of the confining potential includes the screening of the electron field within the QD by the leads.

We have calculated the chemical potential for N electrons confined in the vertical gated QD and found that the chemical potential is a nonlinear function of the gate voltage. We have evaluated the gate-voltage-energy conversion factor, which enabled us to perform a direct comparison of the computational results with the transport-spectroscopy data. For the very small drain-source voltage the calculated positions of the single-electron current peaks on the gate-voltage scale very well agree with the experimental data. In particular, we have quantitatively described the shell filling and Hund's rule for the artificial atoms formed in the vertical gated QD. We have also performed the calculations for the nonzero drain-source voltage, which allowed us to determine the boundaries of the Coulomb diamonds on the stability diagram. We have obtained the positions, sizes, and shapes

of the Coulomb diamonds in very good agreement with experiment.

ACKNOWLEDGMENTS

We are grateful to Leo Kouwenhoven, Guy Austing, and Seigo Tarucha for stimulating discussions and for providing us with the nominal values of the nanostructure parameters. This work was partly supported by the Polish State Committee for Scientific Research (KBN) under Grant No. 5 P03B 04920. One of us (B.S.) gratefully acknowledges the financial support from the Foundation for Polish Science (FNP).

*Email address: adamowski@ftj.agh.edu.pl

[1] P.A. Maksym and T. Chakraborty, Phys. Rev. Lett. **65**, 108 (1990); M.A. Kastner, Phys. Today **46**(1), 24 (1993).

[2] P.L. McEuen, E.B. Foxman, U. Meirav, M.A. Kastner, Y. Meir, N.S. Wingreen, and S.J. Wind, Phys. Rev. Lett. **66**, 1926 (1991); T. Schmidt, M. Tewordt, R.H. Blick, R.J. Haug, D. Pfannkuche, K. von Klitzing, A. Förster, and H. Lüth, Phys. Rev. B **51**, 5570 (1995).

[3] S. Tarucha, D.G. Austing, T. Honda, R.J. van der Hage, and L.P. Kouwenhoven, Phys. Rev. Lett. **77**, 3613 (1996).

[4] L.P. Kouwenhoven, T.H. Oosterkamp, M.W.S. Danoesastro, M. Eto, D.G. Austing, T. Honda, and S. Tarucha, Science **278**, 1788 (1997).

[5] S. De Franceschi, S. Sasaki, J.M. Elzerman, W.G. van der Wiel, S. Tarucha, and L.P. Kouwenhoven, Phys. Rev. Lett. **86**, 878 (2001).

[6] S. Bednarek, B. Szafran, and J. Adamowski, Phys. Rev. B **61**, 4461 (2000).

[7] M. Eto, J. Appl. Phys. **36**, 3924 (1997).

[8] M. Koskinen, M. Manninen, and S.M. Reimann, Phys. Rev. Lett. **79**, 1389 (1997).

[9] T. Ezaki, N. Mori, and C. Hamaguchi, Phys. Rev. B **56**, 6428 (1997).

[10] S. Nagaraja, P. Matagne, V.-Y. Thean, J.-P. Leburton, Y.-H. Kim, and R.M. Martin, Phys. Rev. B **56**, 15 752 (1997).

[11] H. Tamura, Physica B **249-251**, 210 (1998).

[12] O. Steffens, M. Suhrke, and U. Rössler, Physica B **256-258**, 147 (1998).

[13] I.-H. Lee, V. Rao, R.M. Martin, and J.-P. Leburton, Phys. Rev. B **57**, 9035 (1998).

[14] M. Rontani, F. Rossi, F. Manghi, and E. Molinari, Phys. Rev. B **59**, 10 165 (1999).

[15] T.F. Jiang, X.-M. Tong, and S.-I. Chu, Phys. Rev. B **63**, 045317 (2001).

[16] D.G. Austing, T. Honda, and S. Tarucha, Semicond. Sci. Technol. **11**, 388 (1996).

[17] L.P. Kouwenhoven, C.M. Marcus, P.L. McEuen, S. Tarucha, R.M. Westervelt, and N.S. Wingreen, in *Mesoscopic Electron Transport*, Vol. 345 of *NATO Advanced Studies Institute*, edited by L.L. Sohn, L.P. Kouwenhoven, and G. Schön (Kluwer, Dordrecht, 1997), p. 105.

[18] S. Bednarek, B. Szafran, and J. Adamowski, Microelectron. Eng. **51-52**, 99 (2000).

[19] D.G. Austing, T. Honda, Y. Tokura, and S. Tarucha, Jpn. J. Appl. Phys., Part 1 **34**, 1320 (1995); S. Tarucha, D.G. Austing, T. Honda, R. van der Hage, and L.P. Kouwenhoven, *ibid.* **36**, 3917 (1997); L.P. Kouwenhoven, D.G. Austing, and S. Tarucha (private communication).

[20] S. Bednarek, B. Szafran, and J. Adamowski, Phys. Rev. B **59**, 13 036 (1999).

[21] N.A. Bruce and P.A. Maksym, Phys. Rev. B **61**, 4718 (2000).

[22] S. Bednarek and J. Adamowski, Phys. Rev. B **57**, 14 729 (1998).

[23] L.P. Kouwenhoven, N.C. van der Vaart, A.T. Johnson, W. Kool, C.J.P.M. Harmans, J.G. Williamson, A.A.M. Staring, and C.T. Foxon, Z. Phys. B: Condens. Matter **85**, 367 (1991).

[24] J. Weis, R.J. Haug, K. von Klitzing, and K. Ploog, Semicond. Sci. Technol. **9**, 1890 (1994).

[25] J.L. Shen, Y.D. Dai, Y.F. Chen, S.Z. Chang, and S.C. Lee, Phys. Rev. B **51**, 17 648 (1995).

[26] S. Adachi, J. Appl. Phys. **58**, R1 (1985).

[27] D.L. Rode, Phys. Rev. B **2**, 1012 (1970), and Ref. 26.

[28] R.J. Luyken, A. Lorke, M. Haslinger, B.T. Miller, M. Fricke, J.P. Kotthaus, G. Medeiros-Ribeiro, and P.M. Petroff, Physica E (Amsterdam) **2**, 704 (1998).

[29] *Numerical Data and Functional Relationships in Science and Technology*, Landolt-Börnstein, New Series, Group III, Vol. 17, Pt. a, (Springer-Verlag, Berlin, 1982).

[30] R. Colombelli, V. Piazza, A. Badolato, M. Lazzarino, F. Beltram, W. Schoenfeld, and P. Petroff, Appl. Phys. Lett. **76**, 1146 (2000).

[31] J. Adamowski, M. Sobkowicz, B. Szafran, and S. Bednarek, Phys. Rev. B **62**, 4234 (2000).

[32] L.P. Kouwenhoven, D.G. Austing, and S. Tarucha, Rep. Prog. Phys. **64**, 701 (2001).

[33] B. Szafran, J. Adamowski, and S. Bednarek, Physica E (Amsterdam) **5**, 185 (2000).

[34] D.G. Austing, S. Sasaki, S. Tarucha, S.M. Reimann, M. Koskinen, and M. Manninen, Phys. Rev. B **60**, 11 514 (1999).

[35] R.C. Ashoori, H.L. Störmer, J.S. Weiner, L.N. Pfeiffer, S.J. Pearton, K.W. Baldwin, and K.W. West, Phys. Rev. Lett. **68**, 3088 (1992).

[36] S. Tarucha, D.G. Austing, Y. Tokura, W.G. van der Wiel, and L.P. Kouwenhoven, Phys. Rev. Lett. **84**, 2485 (2000).